Absorption and emission of single attosecond light pulses in an autoionizing gaseous medium dressed by a time-delayed control field

Wei-Chun Chu[1] and C. D. Lin[1,2]

[1]*J. R. Macdonald Laboratory, Department of Physics, Kansas State University, Manhattan, Kansas 66506, USA*
[2]*Department of Physics, National Taiwan University, Taipei 10617, Taiwan*

An extreme ultraviolet (EUV) single attosecond pulse passing through a laser-dressed dense gas is studied theoretically. The weak EUV pulse pumps the helium gas from the ground state to the $2s2p(^1P)$ autoionizing state, which is coupled to the $2s^2(^1S)$ autoionizing state by a femtosecond infrared laser with the intensity in the order of 10^{12} W/cm^2. The simulation shows how the transient absorption and emission of the EUV are modified by the coupling laser. A simple analytical expression for the atomic response derived for δ-function pulses reveals the strong modification of the Fano lineshape in the spectra, where these features are quite universal and remain valid for realistic pulse conditions. We further account for the propagation of pulses in the medium and show that the EUV signal at the atomic resonance can be enhanced in the gaseous medium by more than 50% for specifically adjusted laser parameters, and that this enhancement persists as the EUV propagates in the gaseous medium. Our result demonstrates the high-level control of nonlinear optical effects that are achievable with attosecond pulses.

I. INTRODUCTION

The rapidly developing technologies of ultrashort light sources have gained wide applications in the past 10 years [1,2], most notably with the use of attosecond pulses in time-resolved spectroscopy. A typical measurement scheme shines an extreme ultraviolet (EUV) light pulse in the form of an attosecond pulse train (APT) or a single attosecond pulse (SAP) together with a synchronized infrared (IR) laser pulse on an atomic or molecular target and measures the photoions, photoelectrons, or photoabsorption of the EUV. The adjustable time delay between the EUV and the IR gives information of the dynamics of the target. For the SAP in the x-ray regime, this technique has been used to study the emission of Auger electrons [3] in the so-called "streaking" model. Down to the EUV energy, a similar scheme was used to time resolve autoionization where the IR primarily just depleted the resonances excited by the EUV [4,5]. For a SAP at even lower energies, a series of bound states can be excited at once. These states can then be ionized by the IR through different quantum pathways to exhibit interference patterns [6], or dressed by the IR temporarily to exhibit the ac Stark shift [7].

The studies of coupled autoionizing states (AIS) by lasers have been carried out over the past 30 years theoretically [8–11] and experimentally [12]. In these earlier investigations, long pulses were used. For a typical AIS with a lifetime up to tenths of femtoseconds, the coupling lights were considered to be monochromatic, and the measured spectrum was obtained by scanning the photon energy over the widths of the resonances. Not until a few years ago was the same coupling scheme extended to the EUV energy range with femtosecond pulses, where transient absorptions were measured or calculated [13–15]. Very recently, with the emerging attosecond pulses, the timescale of the coupling has been pushed shorter than the decay lifetime of an AIS [4,5] for direct observation in the time domain. In the same scheme, numerous new spectroscopic features were suggested by

simulations [16–21]. Some of these features have been shown recently by experiments with improved energy resolution [22] of the spectrometers. Further technological developments will likely bring more discoveries.

In this work, we focus on resonant laser coupling between two AISs, where a SAP passing through the medium is strongly reshaped in its spectral and temporal distributions by controlling the parameters of the laser and the medium. This reshaping of the SAP, which behaves much beyond what can be described by the simple absorption rate or Beer's law [23], has not been investigated so far. In Ref. [14], the actual propagation of EUV pulses was studied; however, those pulses with durations of tens of femtoseconds are too narrow in bandwidth to demonstrate any meaningful modification in the resonant spectrum. In this study, we look for how a SAP evolves in the medium, which cannot be revealed by a single-atom absorption cross section.

For demonstration at the single-atom model, a 200 as EUV pulse and a time-delayed 9 fs laser pulse are applied to the helium atom. The $2s2p(^1P)$ and $2s^2(^1S)$ AISs are coupled by a 540 nm laser with intensities between 10^{12} and 10^{13} W/cm^2, where the weak EUV excites $2s2p$ from the ground state. For clarity, the pulses are not distinguished as the pump or the probe since they just couple different sets of states. In the single-atom calculation, the electronic wave function, photoelectron, and EUV absorption spectra are carried out for a given set of pulses and atomic parameters. In order to extract the universal features resulting from the coupling, we further derive simple analytic forms of the spectra for short light pulses that are approximated by δ functions in time. This is a valid approximation if the pulse durations are shorter than the atomic timescales, e.g., the 17 fs decay lifetime of $2s2p$. The Fano q parameter [24] preserved in the final forms of the spectra indicates how the population transfer between the AISs is controlled by the coupling and how the wave packet evolves.

For the macroscopic model, the pulses are allowed to propagate through a 2 mm helium gas with number density 8×10^{-3} cm^{-3} (or a pressure of 25 Torr at room temperature). The detected EUV spectra as the pulses exit the medium are calculated. We found that at certain coupling and gas conditions, an enhancement of more than 50% of the incident light at the resonance is produced in the transmission spectrum. This enhancement peak in the frequency domain persists through the propagation where the surrounding background decays along the light path. This demonstrates a remarkable extension of the nonlinear optical control to the attosecond time regime.

II. MODEL

A. Single-atom wave function

In this section, we derive the time-dependent total wave function of a three-level autoionizing system coupled by an EUV pulse and a laser pulse. Two AISs, composed by the bound parts $|b_1\rangle$ and $|b_2\rangle$, and the associated background continua $|E_1\rangle$ and $|E_2\rangle$, respectively, are coupled by the laser, while the $|b_1\rangle$–$|E_1\rangle$ resonance is coupled to the ground state $|g\rangle$ by the EUV; both by dipole transitions. The coupling scheme can be either Ξ type or Λ type. A schematic of the system is in Fig. 1. The pulses are linearly polarized in the same direction and collinearly propagated. The EUV field is expressed by $E_X(t) = F_X(t)e^{i\omega_X t} + F_X^*(t)e^{-i\omega_X t}$ where $F_X(t)$ is the envelope and ω_X is the central frequency of the pulse. The pulse envelope is generally a complex function, which includes all the phase factors in addition to the carrier-frequency terms. The electric field $E_L(t)$ of the laser pulse, however, is kept in the exact form since it may be a few-cycle pulse. The total wave function is in the general form of

$$
\begin{aligned}
|\Psi(t)\rangle = {}& e^{-iE_g t}c_g(t)|g\rangle \\
& + e^{-i(E_g+\omega_X)t}\left[c_{b_1}(t)|b_1\rangle + \int c_{E_1}(t)|E_1\rangle dE_1 \right. \\
& \left. + c_{b_2}(t)|b_2\rangle + \int c_{E_2}(t)|E_2\rangle dE_2 \right].
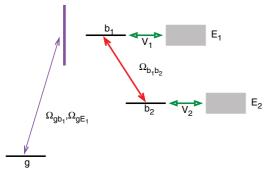\end{aligned}
\tag{1}
$$

FIG. 1. (Color online) Coupling scheme used in the model. The thick red arrow is the laser coupling. The thin purple arrow represents the EUV transition from the ground state to the $|b_1\rangle$–$|E_1\rangle$ resonance, where the bandwidth of the EUV pulse, indicated by the vertical purple line, widely covers the whole lineshape of the resonance. The green arrows with hollow heads are the configuration interactions responsible for the autoionization.

In solving the time-dependent Schrödinger equation (TDSE), we make the following approximations: (1) All the second-order (two-electron) dipole matrix elements, except the resonant excitation $\langle b_1|\mu|g\rangle$ (e.g., the transition between $2s2p$ and $1s^2$), are neglected, i.e., $\langle E_2|\mu|b_1\rangle = \langle b_2|\mu|E_1\rangle = 0$. (2) The rotating wave approximation (RWA) is applied for the EUV coupling (but not the laser coupling) for its high frequency and low intensity. (3) The matrix elements of the Hamiltonian involving $|E_1\rangle$ and $|E_2\rangle$ are independent of energy, where we are only concerned with the energy ranges near the resonances. This means that the target structure is given in terms of the resonance energies E_{b_1} and E_{b_2}, the widths Γ_1 and Γ_2, and the q parameter of the $|b_1\rangle$–$|E_1\rangle$ resonance, which together constitute the basic Fano lineshapes [24]. Note that, with our first approximation, q cannot be defined for the $|b_2\rangle$–$|E_2\rangle$ resonance.

Within the prescribed truncated space, the TDSE for the total wave function in Eq. (1) is reduced to the coupled equations of the coefficients therein, where these coefficients as functions in time should be calculated exactly with the given initial conditions. However, the coefficients associated with the continua, E_1 and E_2, make the calculation less tractable. Thus, we adopt the adiabatic elimination of the continua by assuming that they change much more slowly than the bound states. Then, the approximation $\dot{c}_{E_1}(t) = \dot{c}_{E_2}(t) = 0$ in the coupled equations gives

$$
c_{E_1}(t) = \frac{1}{\delta_1 - \Delta E_1}\left[-F_X^*(t)D_{gE_1}^* c_g(t) + V_1 c_{b_1}(t) \right], \tag{2}
$$

$$
c_{E_2}(t) = \frac{1}{\delta_2 - \Delta E_2}V_2 c_{b_2}(t), \tag{3}
$$

where $\delta_1 \equiv E_X - E_{b_1}$ and $\delta_2 \equiv E_X - E_{b_2}$ are the detuning of the EUV relative to the transitions from the ground state to the AISs, $\Delta E_1 \equiv E_1 - E_a$ and $\Delta E_2 \equiv E_2 - E_b$ are the continuous energies relative to the resonance energies, the Ds are dipole matrix elements, and $V_1 \equiv \langle E_1|H|b_1\rangle$ and $V_2 \equiv \langle E_2|H|b_2\rangle$ are the strengths of the configuration interaction. In return, the coupled equations for the bound state coefficients are reduced to satisfy

$$
i\dot{c}_g(t) = -F_X(t)D_{gb_1}^* \lambda c_{b_1}(t) - i|F_X(t)|^2 j_{gg}c_g(t), \tag{4}
$$

$$
\begin{aligned}
i\dot{c}_{b_1}(t) = {}& -F_X^*(t)D_{gb_1}\lambda c_g(t) - (\delta_1 + i\kappa_1)c_{b_1}(t) \\
& - E_L(t)D_{b_1 b_2}c_{b_2}(t), \tag{5}
\end{aligned}
$$

$$
i\dot{c}_{b_2}(t) = -(\delta_2 + i\kappa_2)c_{b_2}(t) - E_L(t)D_{b_1 b_2}^* c_{b_1}(t), \tag{6}
$$

where $\kappa_1 \equiv \Gamma_1/2$ and $\kappa_2 \equiv \Gamma_2/2$ are half widths of the resonances, $\lambda \equiv 1 - i/q$ represents the transition from the ground state to $|b_1\rangle$ and $|E_1\rangle$ jointly, and $j_{gg} \equiv \pi |D_{gE_1}|^2$ is proportional to the laser broadening. The dipoles (D) in this work are all real numbers since real orbitals are used for the bound states and standing waves are used for the continua. With Eqs. (4)–(6), the bound state part of the wave function is carried out. The procedure so far is identical to what has been employed in the early studies concerning coupled AISs [9–11], except that we do not apply RWA on the laser pulse.

For pulses that are long compared to the resonance lifetime, the pulse bandwidth is narrow, thus each measurement gives the ionization yield at just one single photon energy in

the spectrum. In this case, calculation of the ground-state population $c_g(t)$ described above would be enough for carrying out the ionization spectra. However, in the present study, the bandwidth of the attosecond pulse is broad and can excite the whole AIS, including a significant fraction of the background continuum. The continuum part of the wave function is needed in determining the electron or absorption spectra in a single measurement. Here, the coefficients of the continuum part are retrieved from the original coupled equations

$$i\dot{c}_{E_1}(t) = (E_1 - E_X)c_{E_1}(t) + V_1 c_{b_1}(t) - F_X^*(t)D_{gE_1}^* c_g(t), \tag{7}$$

$$i\dot{c}_{E_2}(t) = (E_2 - E_X)c_{E_2}(t) + V_2 c_{b_2}(t). \tag{8}$$

The retrieval of the continua can be viewed as a "correction" after an iteration from the preliminary forms in Eqs. (2) and (3). Now, the time-dependent total wave function in the form of Eq. (1) is completely solved.

B. Single-atom spectrum

In the following, the electron energy spectrum and photoabsorption spectrum for a single atom are defined by the probability density per unit energy for emitting an electron and for absorbing a photon, respectively. In macroscopic cases where propagation is taken into account, the spectroscopy is expressed in terms of the transmitted light intensity versus the photon energy.

1. Photoelectrons

In standard scattering theory, the atomic scattering waves for momentum $\vec{k}$ are given by

$$\psi_{\vec{k}}(\vec{r}) = \sqrt{\frac{2}{\pi k}}\frac{1}{r}\sum_{lm} i^l e^{i\eta_l} u_l(kr)Y_{lm}(\hat{r})Y_{lm}^*(\hat{k}) \tag{9}$$

in the energy-normalized form, where u_l are real standing wave radial functions, and η_l are the scattering phase shifts. Both u_l and η_l are determined by the atomic potential. If one detects photoelectrons, the momentum distribution will be the projection of the total wave function at a large time onto the scattering waves, i.e.,

$$P(\vec{k}) = \lim_{t\to\infty} |\langle\psi_{\vec{k}}|\Psi(t)\rangle|^2. \tag{10}$$

Likewise, if one measures the energy of the photoelectrons, the spectrum is given by $P(E) = \lim_{t\to\infty} |\langle\psi_E|\Psi(t)\rangle|^2$, where $|\psi_E\rangle$ are the scattering waves for energy E. Remember that $|E_1\rangle$ and $|E_2\rangle$ are conventionally chosen as standing waves, which contains both the incoming and the outgoing components. At large times, since physically the AISs will decay to the continuum, the wave packet will not have incoming components, i.e., the projection onto scattering waves is the same as the projection onto standing waves. Thus, the photoelectron spectra corresponding to the two resonances are simply

$$P_1(E_1) = \lim_{t\to\infty} |c_{E_1}(t)|^2, \quad P_2(E_2) = \lim_{t\to\infty} |c_{E_2}(t)|^2, \tag{11}$$

which require us to calculate the total wave function for a physical time much longer than the decay lifetimes, until $c_{E_1}(t)$ and $c_{E_2}(t)$ stop evolving other than an oscillating phase.

2. Photoabsorption

In a given external field, the total energy absorbed by the atom is

$$\Delta U = \int_0^\infty \omega S(\omega)d\omega, \tag{12}$$

where the response function $S(\omega)$ for $\omega > 0$ represents the absorption probability density and is proportional to the pulse intensity in the frequency domain [14]. Thus, $P(E)$ and $S(\omega)$ have the same dimension and can be directly compared. The absorption cross section $\sigma(\omega)$ is related to $S(\omega)$ by

$$\sigma(\omega) = \frac{4\pi\alpha\omega S(\omega)}{|\tilde{E}(\omega)|^2}, \tag{13}$$

where α is the fine structure constant and $\tilde{E}(\omega)$ is the Fourier transform of the electric field. By considering dipole interactions between the electric field and the atom, $S(\omega)$ is given by

$$S(\omega) = -2\text{Im}[\tilde{\mu}(\omega)\tilde{E}^*(\omega)], \tag{14}$$

where $\tilde{\mu}(\omega)$ is the Fourier transform of the dipole moment.

With the wave function in Eq. (1), the dipole moment is given by

$$\mu(t) = e^{i\omega_X t}u_X(t) + u_L(t) + \text{c.c.}, \tag{15}$$

where the carrier frequency of the EUV has been factored out, and

$$u_X(t) = D_{gb_1}\lambda^* c_{b_1}^*(t)c_g(t) - iF_X(t)j_{gg}|c_g(t)|^2, \tag{16}$$

$$u_L(t) = D_{b_1 b_2} c_{b_2}^*(t)c_{b_1}(t). \tag{17}$$

Note that this model aims to deal with both short- and long-pulse lasers. In the case of a few-cycle laser, the Fourier transform $\tilde{\mu}(\omega)$ at very low frequencies may contain the contributions from both $u_L(t)$ and its complex conjugate, where the separation of the carrier frequency and the envelope is not beneficial; we thus do not employ this separation for the laser pulse in our study.

In a typical ultrafast EUV-plus-IR experiment, the electron or absorption spectra measured over variable time delays between the two pulses are the most common. Photoions are also usually measured, but they do not carry additional information. To study dynamic behavior of autoionization directly in the time domain, light pulses shorter than the typical decay lifetime are necessary. By now few-cycle lasers of durations less than 10 fs are quite common. In the case where both pulses are significantly shorter than any other atomic timescale, major features of the dynamics can be recovered by assuming the pulses are δ functions in time. With this approximation, we are able to reduce the electron and absorption spectra to very simple forms in terms of the pulse areas of the EUV and the laser, the time delay, and the q parameter, where the detailed derivations are shown in the appendix. The modification brought by the laser will have maximum effects when the laser follows the EUV immediately

and its pulse area is $(4N + 2)\pi$ for integer N. In this case the photoelectron distribution flips about the resonance energy. For the light, the absorption line changes to the emission line. These dramatic changes gradually die down when the time delay increases in terms of the decay lifetime of the observed resonance. This δ-pulse analysis will serve to qualitatively explain the result of realistic numerical calculation later in this article.

C. Propagation of light

We have shown how to model the resonance shape of an AIS changed by the strong coupling laser in an atomic system. In principle, both the electron and absorption spectra carry the same essential information, depending on the resonance structure of the states and the laser parameters. However, in electron measurements, high-precision spectroscopy is usually harder to achieve since the lineshape of most Fano resonances requires meV energy resolution. In contrast, such resolution is easier with the transient absorption spectroscopy, as exemplified in a recent report [22]. Thus, in the present work we will put emphasis on absorption spectroscopy.

In a linear medium, the absorption of light is commonly described by Beer's law as

$$T(\omega) = T_0(\omega) \exp\left[-\rho \sigma(\omega) L\right], \tag{18}$$

where $T_0(\omega)$ and $T(\omega)$ are light intensities at the entrance and at the exit of the medium, respectively, ρ is the number density of the particles, $\sigma(\omega)$ is the absorption cross section, and L is the travel distance of light in the medium. This form requires that the cross section has no spatial and temporal dependence and is only a function of energy, and the transmission of light simply decays exponentially with its traveling distance and the gas density. However, in the presence of intense ultrashort IR pulses, the response of the medium can be more complicated, which should be carried out by propagating the exact electric field in the medium.

In the present work, by assuming that the laser is loosely focused, the electric field is a function of time t and the spatial coordinate in the propagation direction z only, where the dependence on the transverse direction is neglected. We assume that the propagation is only forward in z and approximately at the speed of light in vacuum, c. By expressing the time in the moving frame $t' \equiv t - z/c$, the Maxwell equation is reduced to

$$\frac{\partial E(z, t')}{\partial z} = -\frac{\rho}{c\epsilon_0} \frac{\partial \mu(z, t')}{\partial t'}, \tag{19}$$

where ρ is the gas density. Because the EUV and laser frequencies are widely separate, they can be propagated separately. For the EUV, the carrier oscillation terms in field and in dipole are factored out, and the propagation for the field envelope is

$$\frac{\partial F_X(z, t')}{\partial z} = -\frac{\rho}{c\epsilon_0}\left[\frac{\partial u_X(z, t')}{\partial t'} + i\omega_X u_X(z, t')\right]. \tag{20}$$

For the laser, the propagation simply follows Eq. (19) where $\mu(z, t')$ is replaced by $u_L(t') + \text{c.c.}$ The dipole oscillations corresponding to the EUV and laser fields are determined by Eqs. (16) and (17), respectively, and these dipoles determine

how the pulses evolve along z by Eqs. (20) and (19). The TDSE for the single-atom wave function and the Maxwell equation for light propagation are executed sequentially until the pulses exit the medium.

III. RESULTS AND ANALYSIS

In the following, energy and time are expressed in electron volts (eV) and femtoseconds (fs), respectively, and the signal intensities in spectra are expressed in atomic units (a.u.), unless otherwise specified.

A. Results for single atom

In this study, the characteristics of two strongly coupled AISs are demonstrated for neutral helium, the simplest atomic system possessing electron correlation effects. The lowest few AISs in helium are separated from one another on the scale of eVs and are easily coupled by lasers in the near IR to the visible-light energy range. Here we consider a laser pulse [wavelength $\lambda_L = 540$ nm, full width at half maximum (FWHM) duration $\tau_L = 9$ fs, peak intensity $I_L = 2I_0$ where $I_0 \equiv 1$ TW/cm^2 hereafter for convenience] to resonantly couple the $2s2p(^1P)$ and $2s^2(^1S)$ resonances, and a weak EUV SAP (central photon energy $\omega_X = 60$ eV, FWHM duration $\tau_X = 200$ as, peak intensity 10^{10} W/cm^2) to excite $2s2p$ from the ground state by one-photon transition. Both pulse envelopes are in the sine-squared form. The Λ coupling scheme was chosen so that the binding energies of the two AISs are moderately high to prevent ionization by the laser. The time delay t_0 is adjustable, which is defined by the time between the two pulse peaks, and it is positive when the EUV comes first. The broadband EUV covers roughly from 50 to 70 eV and can in principle excite many resonances at once, but due to the choice of the laser wavelength and its relatively narrow bandwidth of about 200 meV, the coupling between the two AISs specified above remains our focus, where it will only be slightly disturbed by the presence of other states if they are not totally negligible.

The time-delayed photoelectron and photoabsorption spectra near the $2s2p$ resonance energy, calculated by the single-atom model, are shown in Figs. 2(a) and 3(a), respectively, for the time delay ranging from -10 fs to 40 fs. Most informative spectral features are included in this range. The resonant coupling laser with intensity $2I_0$ has a pulse area of $1.3 \times 2\pi$, which means that the laser pulse, in its whole, is able to incur Rabi oscillation for 1.3 cycles.

The spectra in Figs. 2(a) and 3(a), calculated with realistic pulse shapes, retain the main features shown in Figs. 7 and 8. The latter two figures are derived analytically by assuming that the two pulses are δ functions in time. The most obvious differences appear when the two pulses overlap, where only the part of the laser after the EUV pulse is responsible for the Rabi oscillation. Unlike the δ-function short pulses, the realistic pulses bring their own timescales into account. Thus, we define an "effective pulse area" by counting only the laser duration after the EUV peak. For $t_0 = 3.5$ fs, the effective pulse area is 2π, i.e., the laser at that time delay supports perfectly a full cycle of Rabi oscillation. In Figs. 2(b) and 3(b), the spectra for $t_0 = 3.5$ fs are plotted. The flipped Fano lineshapes discussed
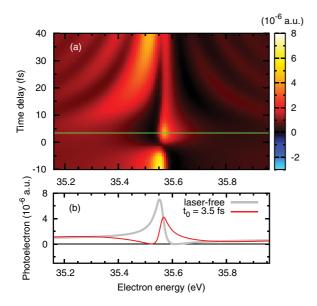
FIG. 2. (Color online) Time-delayed photoelectron spectra near the $2s2p$ resonance excited by a 200 as EUV with a 9 fs laser coupling, calculated by the single-atom model. (a) The spectra between $t_0 = -10$ and 40 fs. The spectra for positive delays are to be compared with those in the δ-pulse analysis in Fig. 7. (b) The spectrum for $t_0 = 3.5$ fs, which corresponds to the green line in panel (a). At this time delay, the resonance profile flips horizontally from the original Fano lineshape, which is shown by the gray curve.

in Sec. II B 2 and in the Appendix are seen. In particular, the electron spectrum flips horizontally where the sign of q is changed, and the absorption spectrum has a upsidedown image, where the absorption peak in the laser-free spectrum points downward, and the signals below the zero line are for the

light emission. These "flipped Fano lineshape" features have been shown in theoretical studies [16–18,20,21] and observed in a recent experiment [22]. While some comprehensive simulations were done previously, the analytical derivation in this work would provide a simple yet effective explanation that could readily be applied.

Note that the AISs decay continuously once they are populated, no matter whether the laser is present or not. For $t_0 = 3.5$ fs, at the time of the laser peak, the $2s2p$ state has already partially autoionized, and the Rabi oscillation is able to affect only electrons that are not autoionized yet. Furthermore, the decay of $2s^2$ also "leaks" some electrons resulting from Rabi oscillation by emitting photoelectrons with its own decay lifetime of 5.3 fs. These factors reduce the distortions that the laser would have imposed on the original Fano lineshape, in both the electron and absorption spectra. As the time delay increases, more electrons are autoionized before the laser and less are coupled by the laser to participate in the Rabi oscillation, and the resonance profile gradually approaches the original Fano lineshape.

While similar three-level coupling schemes have been used for the electromagnetically induced transparency (EIT) effect [25,26], the spectral features in a typical EIT setup, such as the transparency line or Autler-Townes doublet [27], are not recovered by our photoabsorption calculation in Fig. 3. Evidently, the approximation with δ-function pulses breaks down in the long dressing field. To differentiate our mechanism from EIT, we make an additional calculation by keeping all the parameters, but the laser duration is extended from 9 fs to 50 fs. The resultant spectra are plotted in Fig. 4. It shows that the long laser pulse splits the resonance peak into two peaks, with the maximum separation 0.45 eV at $t_0 = 10$ fs. The separation is exactly the Rabi frequency at the laser peak,
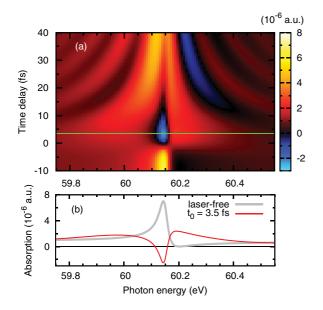

FIG. 3. (Color online) Same as Fig. 2 but for the photoabsorption spectra. The spectra for positive delays are to be compared with the spectra in the δ-pulse analysis in Fig. 8. The resonance profile for $t_0 = 3.5$ fs flips vertically from the original Fano lineshape shown by the gray curve. Note that the negative signals at $t_0 = 3.5$ fs around the resonance energy represent the emission of light. In contrast, the photoelectron spectra in Fig. 2 do not have negative signals.
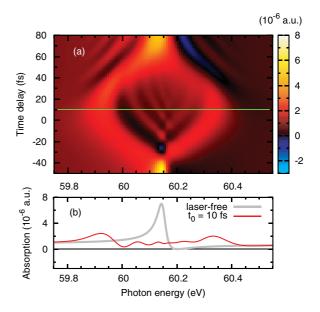

FIG. 4. (Color online) Time-delayed photoabsorption spectra of a 200 as EUV with a 50 fs dressing laser in the single-atom model. (a) The spectra between $t_0 = -50$ fs and 80 fs. The EIT condition is controlled by the time delay between the two pulses. (b) The spectrum for $t_0 = 10$ fs shows the largest separation in the Autler-Townes doublet, which matches the Rabi frequency at the laser peak.

where the Autler-Townes doublet is reproduced. As the time delay changes from this optimal value, the separation decreases and finally drops to 0 for $t_0 < -40$ fs or $t_0 > 70$ fs. It shows that contrary to short dressing pulses, long dressing pulses with many Rabi cycles creates the condition satisfying the "dressed state" picture behind the EIT phenomenon, and the split states appear as expected. By controlling the overlap between the pulses, the doublet can be "turned on" or "turned off." This is the theme of some recent studies applying dressing lasers of tens to hundreds of femtoseconds in an EIT scheme while measuring the time-delayed EUV transmission [13,15,28].

B. Results for gaseous medium

In Sec. III A, the photoabsorption spectrum reveals the appearance of emission line at the resonance for $t_0 = 3.5$ fs. However, it is physically impossible for the light at certain frequency to gain intensity indefinitely when passing through a medium. A realistic pulse has no singularity in the frequency domain. Thus, by intuition, the single-atom result does not represent what will actually be measured in a dense gaseous medium. With the same EUV and laser pulses used in Sec. III A, we consider a gaseous medium made of noninteracting helium atoms with number density $\rho = 8 \times 10^{17}$ cm^{-3} (equivalent to pressure of 25 Torr at room temperature) and thickness $L = 2$ mm, and calculate the transmitted light spectra at the exit of the medium.

The transmitted EUV is plotted in Fig. 5 for three laser intensities, $I_L = 1.1I_0$, $4.5I_0$, and $10I_0$, where I_L is the peak intensity. They safely fall into the intensity range considered by our model. The EUV spectra with overlapping pulses fixed at $t_0 = 0$ are plotted in Fig. 5(a). The effective pulse areas for the three intensities are π, 2π, and 3π, which are responsible for the half, one, and one-and-half cycles of Rabi oscillation. For $1.1I_0$, the spectrum is mostly flat, indicating that while the laser moves the electron population from $2s2p$ to $2s^2$, the $2s2p$ AIS "disappears," leaving only the directly ionized photoelectrons in the vicinity without the hint of autoionization. For $4.5I_0$, the laser drives the electrons back to $2s2p$ with a phase shift of π. The emission line that has been discussed in the single-atom picture is observed here, where the spectral peak appears to be more than 50% of the signal intensity of the incident pulse, which is effectively a partial enhancement of the SAP passing through the gas. When the laser intensifies further to $10I_0$, the Rabi oscillation drives the electrons away from $2s2p$ again; the enhancement is gone, and the spectrum looks flat other than a slight bump. These three laser intensities demonstrate how the number of cycles in the Rabi oscillation controls the phase of the $2s2p$ AIS, which then determines the resonance lineshape at the end of the autoionization.

The presentation in Fig. 5(a) is for the overlapping pulses, i.e., the Rabi oscillation happens within the laser duration at the beginning of the 17 fs decay of $2s2p$. It is a simplified case where autoionization occurs approximately after the population transfer by the laser is done. However, for larger time delays, the laser comes after $2s2p$ decays for some time and only affects the later part of the decay. The total wave packet is the coherent sum of autoionization before the laser, and the quantum path going through the Rabi oscillation. In Fig. 5(b), the total signal yields in the 50 meV range around
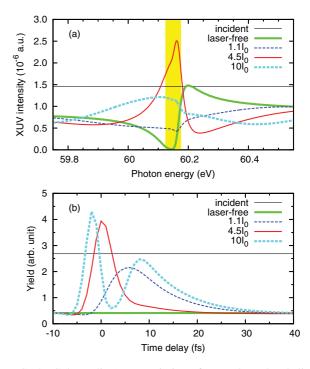

FIG. 5. (Color online) Transmission of EUV through a helium gaseous medium dressed by a 9 fs laser of peak intensities (I_L) of 0 (laser free), $1.1I_0$, $4.5I_0$, and $10I_0$. The incident light is plotted as a reference. (a) Transmitted EUV profiles for overlapping pulses ($t_0 = 0$), where the effective pulse areas of the laser are 0, π, 2π, and 3π. The flipping of the resonance profile is predicted as the main feature by the single-atom case, although more structures are seen here. The signal at the resonance for $I_L = 4.5I_0$ is enhanced significantly, with more than 50% increase from the incident light. This measurable quantity can only be obtained by applying field propagation. (b) Total photon signals (yield) gathered in the 50 meV energy range at the resonance [indicated in panel (a) by the yellow vertical stripe] as functions of the time delay. This energy range complies with the spectrometer resolution under current technology. The yield for each laser intensity oscillates with the time delay, which shows a high degree of control in the time domain.

the $2s2p$ resonance for different intensities and time delays are plotted. This plot is equivalent to a measurement of the EUV signal at the resonance energy with a spectrometer of 50 meV resolution in order to investigate the enhancement. For each intensity, the yield oscillates with the time delay. As seen in the figure, $4.5I_0$ is no longer the definite optimal intensity to enhance the transmitted SAP resonance. For example, when the $10I_0$ pulse is at $t_0 = -2$ fs, the enhancement is higher than what can be achieved by the $4.5I_0$ pulse. This is because even when both intensities have the same effective pulse area, the $10I_0$ pulse accomplishes the Rabi oscillation in a slightly earlier stage in the decay of $2s2p$, where less electrons escape its influence by autoionization. It is very remarkable that this partial enhancement of a SAP is controlled within an energy scale of about 100 meV in the form of resonance lineshape, and within a timescale of about 1 fs in the form of time delay.

It has been demonstrated in Fig. 5(a) that while the resonance lineshape of the EUV pulse is controlled by the laser coupling, the spectral profile away from the resonance energy always drops in light transmission spectroscopy. It is
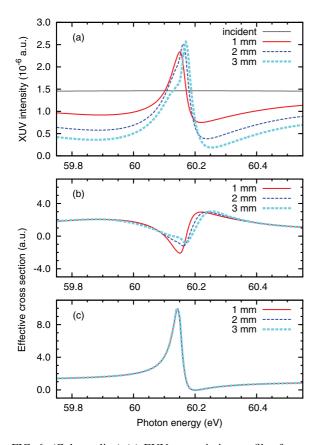
FIG. 6. (Color online) (a) EUV transmission profiles for propagation lengths $L = 1$, 2, and 3 mm in the gaseous medium with the overlapping 9 fs, $4.5I_0$ dressing laser pulse. When the dressing laser is turned on, the enhanced peak persists while the surrounding background attenuates. Panels (b) and (c) show effective absorption cross sections $\sigma_{\rm eff}(\omega)$ for the same propagation lengths as in panel (a) with and without the dressing laser, respectively. With the dressing laser, $\sigma_{\rm eff}(\omega)$ changes with L at the resonance but stays the same in the outside region. Without the dressing field, $\sigma_{\rm eff}(\omega)$ over the whole energy range does not change with L, where Beer's law applies. The contrast between the cases with and without the dressing laser demonstrates a strong nonlinear response of the gas to the laser field which is reflected in the transmission of the attosecond pulse.

imaginable that the overall light attenuates when propagating in the gas. It is thus very intriguing to know how the exceptional enhanced resonance peak holds its shape and strength in the propagation. In Fig. 6, we show the transmitted EUV spectra at different distances along the beam path with the 9 fs, $4.5I_0$ dressing pulse at 0 time delay. The transmitted EUV intensities and the corresponding effective absorption cross sections, defined by [see Eq. (18)]

$$\sigma_{\rm eff}(\omega) \equiv -\frac{1}{\rho L} \ln \frac{T(\omega)}{T_0(\omega)}, \qquad (21)$$

are shown in Figs. 6(a) and 6(b), respectively. With such laser parameters, the "wings" on the two sides of the resonance profile descend, but the enhancement peak is up to about 50% of the incident intensity and roughly maintains its height from 1 to 3 mm. The persistence of the enhancement peak, apart from the exponential decay of the rest of the signals along the propagation, displays an impressive nonlinear response of the

gas to the laser pulse. This violation to Beer's law is in a very selective energy range and is sensitive to the parameters of the dressing laser. To elucidate the nonlinearity of the dressing laser, $\sigma_{\rm eff}(\omega)$ without the dressing field is plotted in Fig. 6(c). In this case, the propagation of the EUV actually follows Beer's law stated in Eq. (18), where the cross section determined by the original Fano lineshape remains the same over the distance. The pulse over the whole energy range is absorbed indifferently.

IV. CONCLUSION

A three-level autoionizing system coupled by a SAP and a time-delayed intense femtosecond laser have been modeled. The photoelectron and photoabsorption spectra are responsive most obviously to the laser intensity and its time delay. We analyze the spectra by assuming both pulses are infinitely short, where the responses can be explained by the precise control of the Rabi oscillation between the two AISs. The analysis also suggests that the phase change in the wave packet during the Rabi oscillation is mapped out in the flipping of the Fano lineshape. The model calculation with realistic pulse parameters also produces these significant features. In contrast, with long dressing fields, these spectral features are replaced by the Autler-Townes doublet, which is well studied in systems coupled by stable lasers. This contrast demonstrates that the ultrashort coupling demolishes the dressed-state picture, and the dynamics of the system is better viewed directly in the time domain.

Focusing on the response of the SAP light in this coupled system, we further incorporate the single-atom response with the pulse propagation in the gaseous medium. The main controllable features of the resonance profile shown by a single atom are well preserved in the gaseous medium. By applying a laser pulse with a 2π effective pulse area to couple the $2s2p$ and $2s^2$ resonances in the dense helium gas, an enhanced peak at the $2s2p$ resonance shows up in the transmitted SAP spectrum, where the signal intensity retains more than 50% gain from the entrance to the exit of the medium. At the same time, the signals away from the resonance energy drops along the propagation as described by Beer's law. It can be viewed as the pulse shaping of a SAP that is measurable in the energy domain. This result illustrates a strong nonlinear manipulation of a SAP by an ultrafast dressing field, which would open new possibilities of control of attosecond dynamics.

APPENDIX: ATOMIC RESPONSE IN SHORT-PULSE LIMIT

In the short-pulse limit, we assume that the field envelopes are rectangular with given carrier frequencies. As the durations

approach zero, the envelopes are

$$F_X(t) = \frac{A_X}{2} D_{gb_1} \delta(t), \quad F_L(t) = \frac{A_L}{2} D_{b_1 b_2} \delta(t - t_0), \quad \text{(A1)}$$

where A_X and A_L are equivalent to the pulse areas for the EUV and laser, respectively, and t_0 is the time delay between the pulse peaks, which is positive when the EUV comes first. Since the intensity of the laser is not enough to excite the atom from the ground state, we only consider the time delay $t_0 \geqslant 0$. The infinitely short pulses cut the time into regions where the TDSE in each region can be solved analytically. The EUV is weak so that perturbation is applied on its transition. In order to observe the universal features of the electron and absorption spectra regardless of the atomic parameters, the energy is scaled by $\epsilon \equiv 2(E - E_{b_1})/\Gamma_1$, where Γ_1 is the resonance width (see Sec. II). Note that now E_{b_1} represents either the electron energy or the photon energy depending on whether we look at the electron or absorption spectra. This scaling is the same as Fano's characterization of resonances [24]. The time delay is scaled by $\tau \equiv \Gamma_1 t_0/2$.

With some algebra, the electron spectrum is found to be given by

$$P(\epsilon) = \frac{|A_X|^2}{1 + \epsilon^2} [(q + \epsilon)^2 - c e^{-\tau} f_P(\epsilon)], \quad \text{(A2)}$$

where

$$c \equiv 1 - \cos(A_L/2) \quad \text{(A3)}$$

and

$$f_P(\epsilon) \equiv 2(q + \epsilon)[q \cos(\epsilon \tau) + \sin(\epsilon \tau)] + c e^{-\tau}(q^2 + 1). \quad \text{(A4)}$$

Similarly, the absorption spectrum is given by

$$S(\epsilon) = \frac{|A_X|^2}{1 + \epsilon^2} [(q + \epsilon)^2 - c e^{-\tau} f_S(\epsilon)], \quad \text{(A5)}$$

where

$$f_S(\epsilon) \equiv (q^2 - 1 + 2q\epsilon) \cos(\epsilon \tau) + [2q + (1 - q^2)\epsilon] \sin(\epsilon \tau). \quad \text{(A6)}$$

Both spectra are composed of two terms. The first term is the original Fano lineshape defined by the $|b_1\rangle$–$|E_1\rangle$ resonance alone, without any influence from the laser. The second term decays exponentially with the time delay τ and is proportional to the coefficient c determined by the laser pulse area A_L as defined by Eq. (A3). The minimum value of c is 0, which corresponds to $A_L = 0, 4\pi, 8\pi, \ldots$, where the Rabi oscillation has even number of cycles. In this condition, the electrons coming back to $|b_1\rangle$ carry no additional phase, and the laser effectively does nothing. On the contrary, the maximum value of c, 2, corresponds to $A_L = 2\pi, 6\pi, 10\pi, \ldots$ and an odd number of cycles. The returning electrons have additional phase of π.

In order to demonstrate the influence of laser strength more clearly, the electron and absorption time-delayed spectra for $A_L = 2\pi$ are plotted in Figs. 7 and 8, respectively. As seen in both figures, when τ is large, very little change is brought by the laser onto the original Fano lineshape. However, in the $\tau \to 0$ limit, the electron spectrum flips in the energy
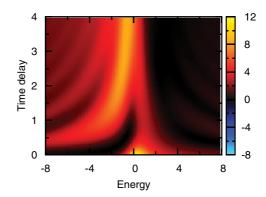

FIG. 7. (Color online) Photoelectron spectra with infinitely short pulses, as described by Eq. (A2). The energy is scaled by $\Gamma_1/2$, and the time delay is scaled by $2/\Gamma_1$. The pulse area of laser is $A_L = 2\pi$, which indicates a full cycle of Rabi oscillation by the laser coupling. When the time delay is large, the spectrum approaches the original Fano lineshape. When the time delay is 0, the spectrum is close to a horizontally flipped image of the original Fano lineshape.

dimension around $\epsilon = 0$, and the absorption spectrum displays a strong emission line near $\epsilon = 0$.

The significant change of spectral features at $\tau = 0$ can be expressed analytically by reducing Eqs. (A2) and (A5) to

$$P(\epsilon) = |A_X|^2 \frac{(-q + \epsilon)^2 + 4}{1 + \epsilon^2}, \quad \text{(A7)}$$

$$S(\epsilon) = |A_X|^2 \left[-\frac{(q + \epsilon)^2}{1 + \epsilon^2} + 2 \right]. \quad \text{(A8)}$$

In the electron spectrum, the mirror image of Fano resonance, indicated by the minus sign of the q parameter, is added onto a Lorentzian shape. In the absorption spectrum, beside an additional constant background, the whole resonance function flips upsidedown, which means that the absorption line becomes the emission line. Note that Eqs. (A7) and (A8) are the results for a full Rabi cycle and represent the extreme changes that the strong coupling can bring. For noninteger number of cycles, among the two resonances, some electrons will stay at $|b_2\rangle$ at the end of the laser and will not be combined with the photoelectrons in the neighborhood of $|b_1\rangle$.
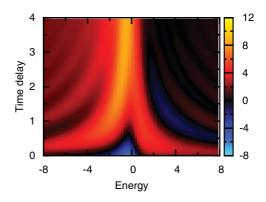

FIG. 8. (Color online) Same as Fig. 7 but for the photoabsorption, as described by Eq. (A6). When the time delay is 0, the spectrum is close to a vertically flipped image of the original Fano lineshape.

[1] F. Krausz and M. Ivanov, Rev. Mod. Phys. **81**, 163 (2009).

[2] G. Sanone, L. Poletto, and M. Nisoli, Nat. Photonics **5**, 655 (2011).

[3] M. Drescher, M. Hentschel, R. Kienberger, M. Uiberacker, V. Yakovlev, A. Scrinzi, Th. Westerwalbesloh, U. Kleineberg, U. Heinzmann, and F. Krausz, Nature (London) **419**, 803 (2002).

[4] H. Wang, M. Chini, S. Chen, C.-H. Zhang, F. He, Y. Cheng, Y. Wu, U. Thumm, and Z. Chang, Phys. Rev. Lett. **105**, 143002 (2010).

[5] S. Gilbertson, M. Chini, X. Feng, S. Khan, Y. Wu, and Z. Chang, Phys. Rev. Lett. **105**, 263003 (2010).

[6] J. Mauritsson *et al.*, Phys. Rev. Lett. **105**, 053001 (2010).

[7] M. Chini, B. Zhao, H. Wang, Y. Cheng, S. X. Hu, and Z. Chang, Phys. Rev. Lett. **109**, 073601 (2012).

[8] P. Lambropoulos and P. Zoller, Phys. Rev. A **24**, 379 (1981).

[9] H. Bachau, P. Lambropoulos, and R. Shakeshaft, Phy. Rev. A **34**, 4785 (1986).

[10] L. B. Madsen, P. Schlagheck, and P. Lambropoulos, Phys. Rev. Lett. **85**, 42 (2000).

[11] S. I. Themelis, P. Lambropoulos, and M. Meyer, J. Phys. B: At., Mol. Opt. Phys. **37**, 4281 (2004).

[12] N. E. Karapanagioti, O. Faucher, Y. L. Shao, D. Charalambidis, H. Bachau, and E. Cormier, Phys. Rev. Lett. **74**, 2431 (1995).

[13] Z. H. Loh, C. H. Greene, and S. R. Leone, Chem. Phys. **350**, 7 (2008).

[14] M. B. Gaarde, C. Buth, J. L. Tate, and K. J. Schafer, Phys. Rev. A **83**, 013419 (2011).

[15] M. Tarana and C. H. Greene, Phys. Rev. A **85**, 013411 (2012).

[16] W.-C. Chu, S.-F. Zhao, and C. D. Lin, Phys. Rev. A **84**, 033426 (2011).

[17] W.-C. Chu and C. D. Lin, Phys. Rev. A **85**, 013409 (2012).

[18] J. Zhao and M. Lein, New J. Phys. **14**, 065003 (2012).

[19] A. N. Pfeiffer and S. R. Leone, Phys. Rev. A **85**, 053422 (2012).

[20] W.-C. Chu and C. D. Lin, J. Phys. B: At., Mol. Opt. Phys. **45**, 201002 (2012).

[21] L. Argenti, C. Ott, T. Pfeifer, and F. Martín, arXiv:1211.2526.

[22] C. Ott, A. Kaldun, P. Raith, K. Meyer, M. Laux, Y. Zhang, S. Hagstotz, T. Ding, R. Heck, and T. Pfeifer, arXiv:1205.0519.

[23] A. Ishimaru, *Wave Propagation and Scattering in Random Media* (IEEE, New York, 1997), Chap. 6.

[24] U. Fano, Phys. Rev. **124**, 1866 (1961).

[25] S. E. Harris, J. E. Field, and A. Imamoglu, Phys. Rev. Lett. **64**, 1107 (1990).

[26] M. Fleischhauer, A. Imamoglu, and J. P. Marangos, Rev. Mod. Phys. **77**, 633 (2005).

[27] S. H. Autler and C. H. Townes, Phys. Rev. **100**, 703 (1955).

[28] T. E. Glover *et al.*, Nat. Phys. **6**, 69 (2010).